# Supporting Information

## Magnetic Hollow Spheres Assembled from Graphene-Encapsulated Nickel Nanoparticles for Efficient Photocatalytic $CO_2$ Reduction

Xiahui Lin,[†,‡] Sibo Wang,[‡] Wenguang Tu,[‡] Haojing Wang,[‡] Yidong Hou,[†] Wenxin Dai,*[,†] and Rong Xu*[,‡]

[†] State Key Laboratory of Photocatalysis on Energy and Environment, Fuzhou University, Fuzhou 350002, China

[‡] School of Chemical and Biomedical Engineering, Nanyang Technological University, 62 Nanyang Drive, Singapore 637459, Singapore

* Corresponding authors. Email: daiwenxin@fzu.edu.cn; rxu@ntu.edu.sg;

**Characterizations:** The morphologies and structures of the samples were characterized with field-emission scanning electron microscopy (FESEM; JEOL JSM 6700) and transmission electron microscopy (TEM; JEOL 3010). The chemical composition of the samples were analysed by EDX attached to JSM 6701F. The X-ray diffraction (XRD) patterns of the as-prepared samples were obtained on a X-ray diffractometer (Bruker D2 Phase, Cu Kα). Raman spectra were collected in a Renishaw InVia Reflex Raman with a 514 nm excitation wavelength. The $N_2$ and the $CO_2$ sorption measurements were carried out on an ASAP2020M analyser at 77 and 273 K, respectively. X-ray photoelectron spectroscopy (XPS) characterizations were performed on a PHI Quantum 2000 XPS system with a monochromatic Al Kα source and a charge neutralizer. All XPS peaks were calibrated against the C1s signal of contaminant carbon at a binding energy of 284.6 eV. The ICP-OES tests were performed on Agilent 720 ICP-OES. Photoluminescence (PL) tests for the reaction mixtures were conducted with and without addition of the catalyst under light irradiation on Edinburgh Analytical Instruments FL/FSTCSPC920 coupled with a time-correlated single-photo-counting system at room temperature. The photocurrent measurements were conducted in the reaction mixtures with and without the Ni@GC catalyst using a CHI 660E electrochemical workstation in a typical three-electrode system: the ITO glass as the working electrode, the Pt net as the counter electrode and an Ag/AgCl electrode as the reference electrode.

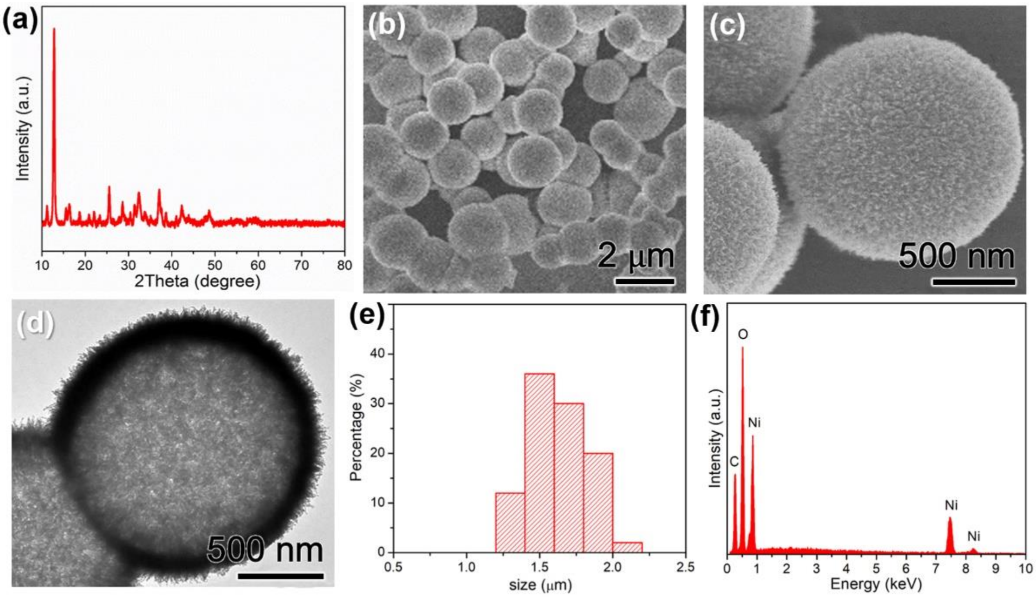


**Figure S1.** (a) XRD pattern, (b, c) FESEM images, (d) TEM image, (e) size distribution plot and (f) EDX spectrum of the Ni-MOF spheres.

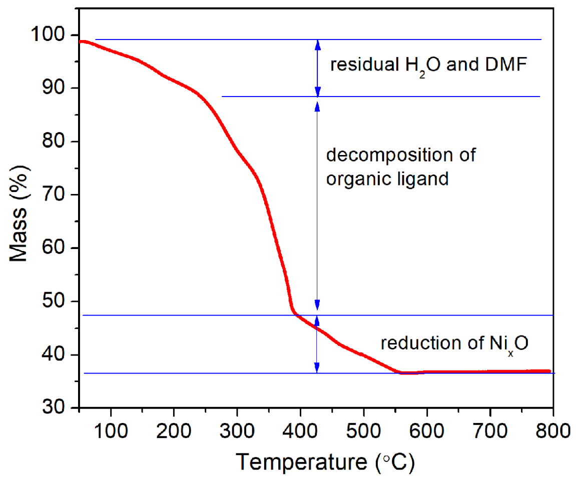


**Figure S2.** TGA results of Ni-MOF in a $N_2$ atmosphere with a heating rate of 5 ºC $min^{-1}$.

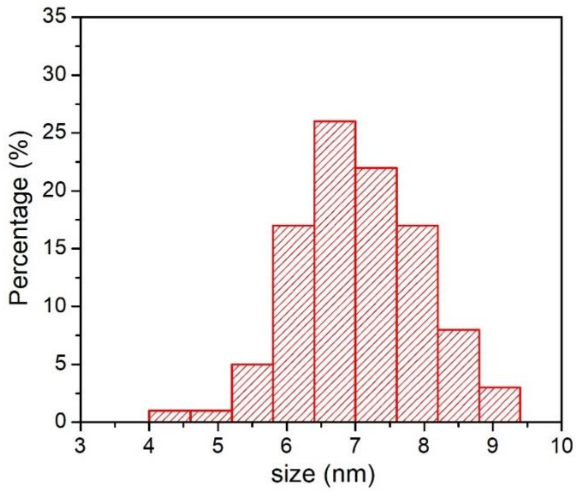


**Figure S3.** The Ni size distribution plot of Ni@GC.

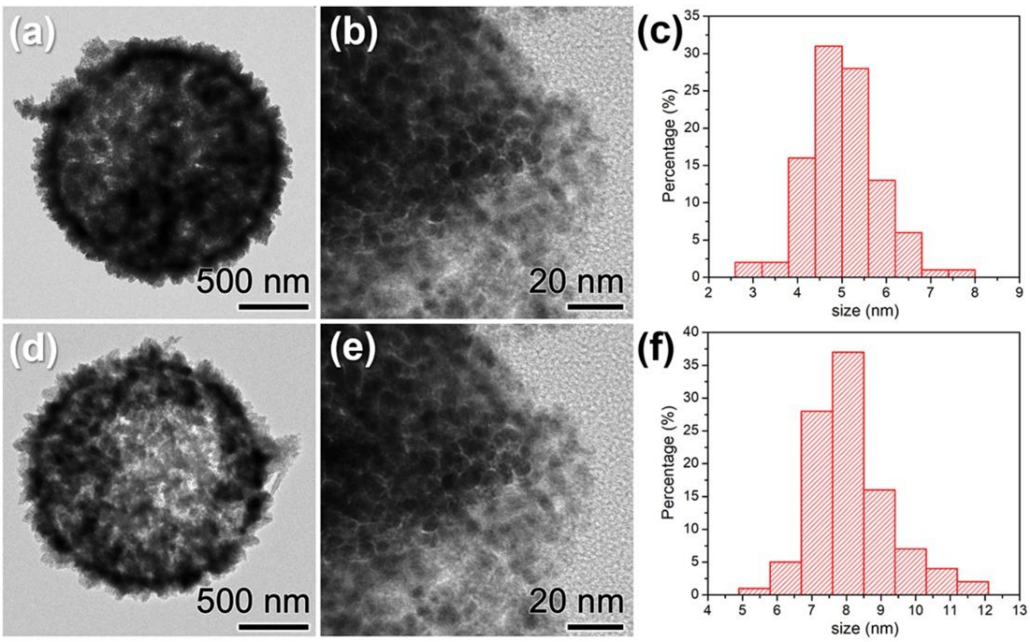


**Figure S4.** (a,b,d,e) TEM images and (c,f) the corresponding Ni size distribution plots of (a-c) Ni@GC-500 and (d-f) Ni@GC-700.

of chemisorbed $CO_2$ at relatively high temperature.

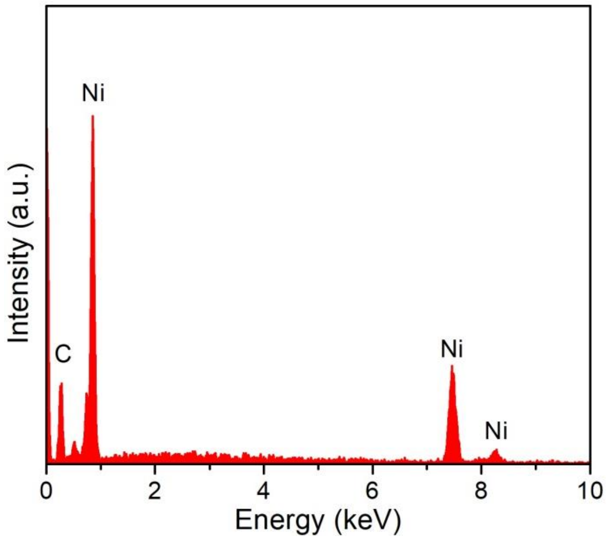


**Figure S5.** EDX spectrum of Ni@GC.

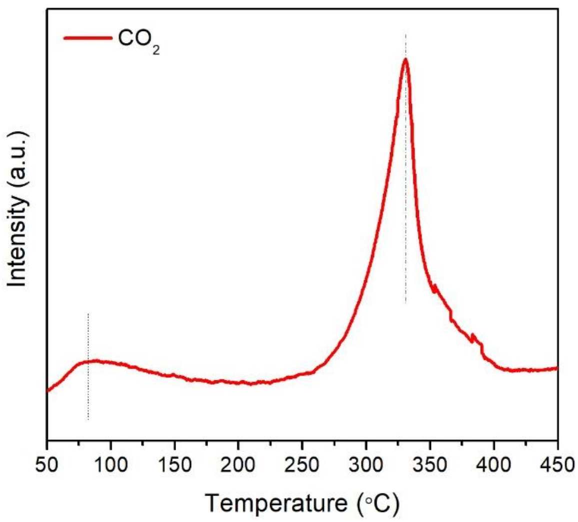


**Figure S6.** $CO_2$-TPD profile of Ni@GC catalyst. The signal peak at 86 °C is attributed to the desorption of physically adsorbed $CO_2$, while the other peak at 330 °C corresponds to the desorption of chemisorbed $CO_2$.

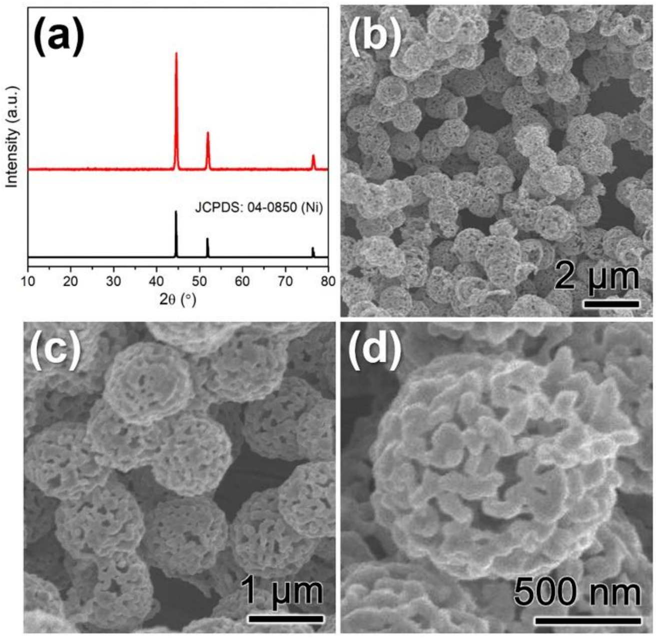


**Figure S7.** (a) XRD pattern and (b-d) FESEM images of Ni NPs.

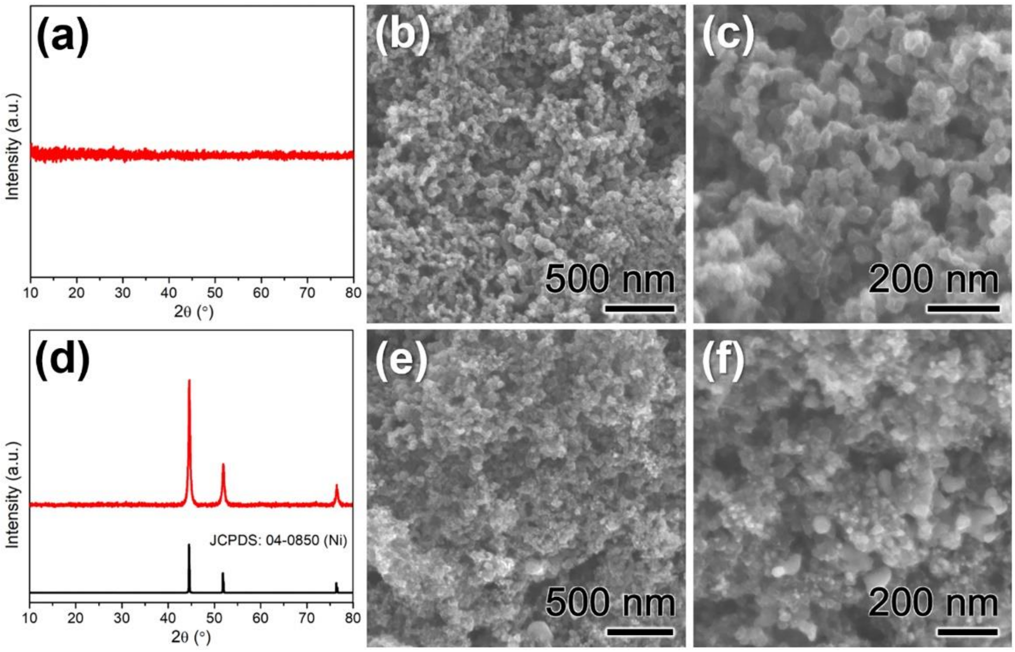


**Figure S8.** (a) XRD pattern and (b,c) FESEM images of graphite carbon support. (d) XRD pattern and (e,f) FESEM images of the Ni/GC catalyst.

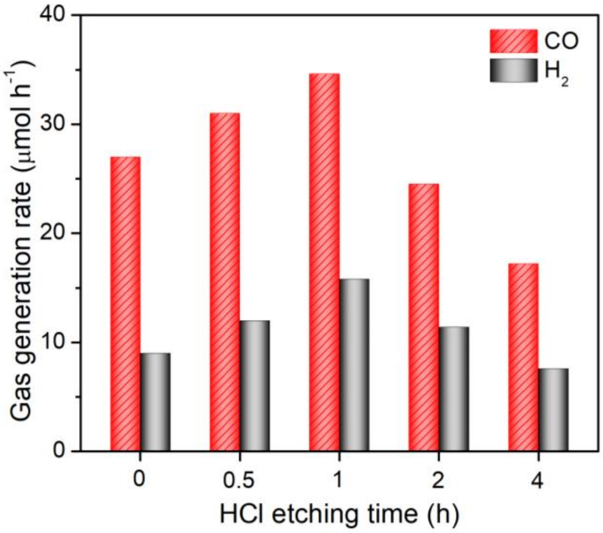


**Figure S9.** Photocatalytic $CO_2$ reduction performance of the Ni@GC catalysts after etching in 4 M HCl solution at room temperature for different durations. The reaction conditions were kept the same as those stated in the caption of Figure 5d.

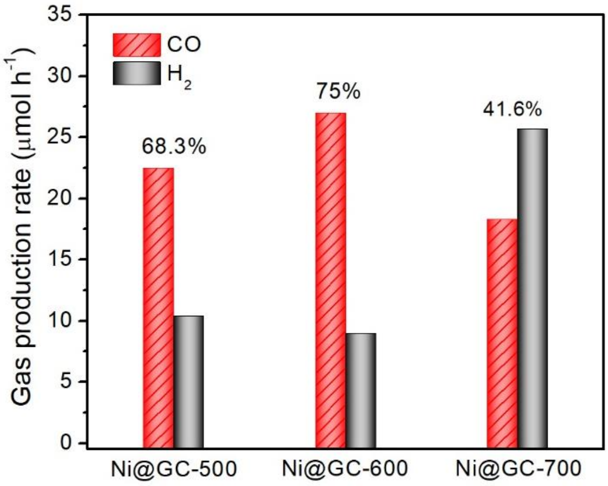


**Figure S10.** Photocatalytic $CO_2$ reduction activity of the Ni@GC-500, Ni@GC and Ni@GC-700 samples. The percentage refers to the corresponding CO selectivity of the samples.

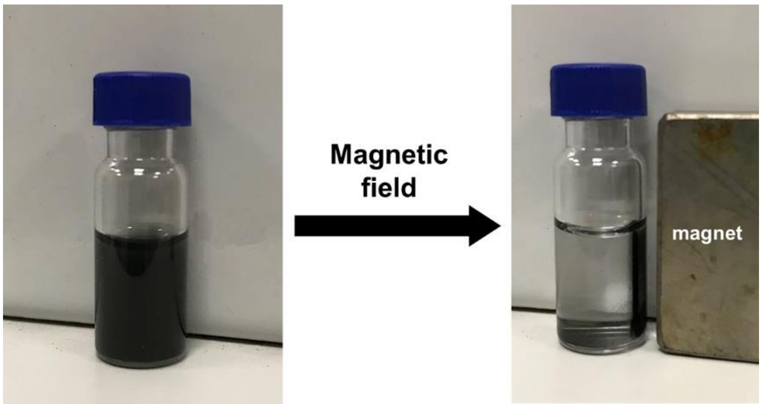


**Figure S11.** Photographs showing the separation of the Ni@GC catalyst by using an external magnet.

**Table S1.** Comparison of photocatalytic $CO_2$ reduction performance of Ni@GC with some catalysts reported recently in similar reaction systems under visible light irradiation ($\lambda > 420$ nm).

| Catalyst | Photosensitizer<br>Sacrificial agent | Product-releasing rate ($\mu mol\ h^{-1}$) | $CO_2$ reduction Selectivity (%) | Stability | Refs. |
|---|---|---|---|---|---|
| Ni@GC | $Ru(bpy)_3^{2+}$<br>TEOA | CO: 27<br>$H_2$: 9<br>After acid treatment: CO: 35<br>$H_2$: 16 | 75.0<br><br>68.6 | 5 repeats, almost unchanged | This work |
| $Co_3O_4$ | $Ru(bpy)_3^{2+}$<br>TEOA | CO: 35.2<br>$H_2$: 10.5 | 77.1 | 5 repeats, ~5% decrease | 1 |
| Co-ZIF-9 | $Ru(bpy)_3^{2+}$<br>TEOA | CO: 41.8<br>$H_2$: 29.9 | 58.3 | 5 repeats, almost unchanged | 2 |
| CdS QD | $[Ni(terpy)_2]^{2+}$<br>TEOA | CO: 11.43<br>$H_2$: 1 | 92.0 | N/A[i] | 3 |
| Ni(TPA/TEG) | $Ru(bpy)_3^{2+}$<br>TEOA | CO: 26.6 | *ca.* 100 | 5 repeats, ~5% decrease | 4 |
| $Ni_3(HITP)_2$ | $Ru(bpy)_3^{2+}$<br>TEOA | CO: 69<br>$H_2$: 2.1 | 97.0 | N/A | 5 |
| Co/C | $Ru(bpy)_3^{2+}$<br>TEOA | CO: 22.4<br>$H_2$: 12.6 | 64.2 | 3 repeats, 10% decrease | 6 |
| $CoSn(OH)_6$ | $Ru(bpy)_3^{2+}$<br>TEOA | CO: 18.7<br>$H_2$: 3.0 | 86.2 | 5 repeats, ~5% decrease | 7 |
| Ni MOLs[ii] | $Ru(bpy)_3^{2+}$<br>TEOA | CO: 12.5<br>$H_2$: 0.28 | 97.8 | N/A | 8 |
| $NC@NiCo_2O_4$ | $Ru(bpy)_3^{2+}$<br>TEOA | CO: 26.2<br>$H_2$: 3.4 | 88.6 | 5 repeats, almost unchanged | 9 |
| $CuInS_2/ZnS$[iii] | FeTPP<br>DMSO | CO: 11.2<br>$H_2$: 2.2 | 83.6 | N/A | 10 |

[i]N/A: not available; [ii]Ni MOLs: Ni metal-organic framework monolayers; [iii] $\lambda = 450$ nm.

## References


(1) Gao, C.; Meng, Q.; Zhao, K.; Yin, H.; Wang, D.; Guo, J.; Zhao, S.; Chang, L.; He, M.; Li, Q. $Co_3O_4$ Hexagonal Platelets with Controllable Facets Enabling Highly Efficient Visible-Light Photocatalytic Reduction of $CO_2$. *Adv. Mater.* **2016,** *28* (30), 6485.

(2) Wang, S.; Yao, W.; Lin, J.; Ding, Z.; Wang, X. Cobalt Imidazolate Metal–Organic Frameworks Photosplit $CO_2$ under Mild Reaction Conditions. *Angew. Chem. Int. Ed.* **2014,** *53* (4), 1034.

(3) Kuehnel, M. F.; Orchard, K. L.; Dalle, K. E.; Reisner, E. Selective Photocatalytic $CO_2$ Reduction in Water through Anchoring of a Molecular Ni Catalyst on CdS Nanocrystals. *J. Am. Chem. Soc.* **2017,** *139* (21), 7217.

(4) Niu, K.; Xu, Y.; Wang, H.; Ye, R.; Xin, H. L.; Lin, F.; Tian, C.; Lum, Y.; Bustillo, K. C.; Doeff, M. M.et al. A spongy nickel-organic $CO_2$ reduction photocatalyst for nearly 100% selective CO production. *Sci. Adv.* **2017,** *3* (7), e1700921.

(5) Zhu, W.; Zhang, C.; Li, Q.; Xiong, L.; Chen, R.; Wan, X.; Wang, Z.; Chen, W.; Deng, Z.; Peng, Y. Selective reduction of $CO_2$ by conductive MOF nanosheets as an efficient co-catalyst under visible light illumination. *Appl. Catal. B Environ.* **2018,** *238*, 339.

(6) Zhao, K.; Zhao, S.; Gao, C.; Qi, J.; Yin, H.; Wei, D.; Mideksa, M. F.; Wang, X.; Gao, Y.; Tang, Z.et al. Metallic Cobalt–Carbon Composite as Recyclable and Robust Magnetic Photocatalyst for Efficient $CO_2$ Reduction. *Small* **2018,** *14* (33), 1800762.

(7) Lin, X.; Gao, Y.; Jiang, M.; Zhang, Y.; Hou, Y.; Dai, W.; Wang, S.; Ding, Z. Photocatalytic $CO_2$ reduction promoted by uniform perovskite hydroxide $CoSn(OH)_6$ nanocubes. *Appl. Catal. B Environ.* **2018,** *224*, 1009.

(8) Han, B.; Ou, X.; Deng, Z.; Song, Y.; Tian, C.; Deng, H.; Xu, Y. J.; Lin, Z. Nickel Metal–Organic Framework Monolayers for Photoreduction of Diluted $CO_2$: Metal-Node-Dependent Activity and Selectivity. *Angew. Chem. Int. Ed.* **2018,** *57* (51), 16811.

(9) Wang, S.; Guan, B. Y.; Lou, X. W. Rationally designed hierarchical N-doped carbon@$NiCo_2O_4$ double-shelled nanoboxes for enhanced visible light $CO_2$ reduction. *Energy Environ. Sci.* **2018,** *11* (2), 306.

(10) Lian, S.; Kodaimati, M. S.; Dolzhnikov, D. S.; Calzada, R.; Weiss, E. A. Powering a $CO_2$ Reduction Catalyst with Visible Light through Multiple Sub-picosecond Electron Transfers from a Quantum Dot. *J. Am. Chem. Soc.* **2017,** *139* (26), 8931.